

University of Reading

The Position of the Free Boundary Formed Between an Expanding Plasma and an Electric Field in Differing Geometries

Peter Spence

August 2003

Submitted to the Department of Mathematics, University of Reading, in partial fulfilment of the requirements for the Degree of Master of Science.

Abstract

The problem of determining the position of the boundary formed between a plasma expanding into an evacuated region (subject to a large electric field) and the vacuum itself has been formulated. The problem has been solved in an analytical manner for the simple 1D planar case, and solutions to this problem have been analysed. A different iterative method of solving the same problem based on nodal equidistribution has been formulated and successfully implemented, and solutions compared with the analytic case. The same iterative method has also been successfully applied to the more difficult 1D radially symmetric problem and the effects of solution gradient and an input parameter γ on nodal distribution have been studied.

Declaration

I confirm that this is my own work and the use of all material from other sources has been properly and fully acknowledged.

©Crown Copyright 2003

"This document is of United Kingdom origin and contains proprietary information which is the property of the Secretary of State for Defence. It is furnished in confidence and may not be copied, used or disclosed in whole or in part, without prior written consent of the Director of Commercial & Defence Procurement Agency, Ash 2b, Mailpoint 88, MOD, Abbey Wood, Bristol, BS34 8JH, England."

Contents

1	Introduction	6
1.1	Neutron Tube Basic Operation	6
1.2	Free Boundary Problem	8
1.3	Solution Approach	9
2	1D Planar Case	10
2.1	Analytic Solution	11
2.2	Results from Analytic Solution	12
2.2.1	Change in Solution Region Size with Current Density .	14
2.2.2	Change in Solution Region Size with Accelerating Voltage	15
2.2.3	Predicted Solution Region Size for a Typical Neutron Tube	16
2.3	Equidistribution Method	17
2.4	Introduction of Pseudo Time	18
2.5	Mapping from Physical Grid to Logical Grid	19
2.6	Choice of Monitor Function	21
2.6.1	Equally Distributed Nodes ($M = 1$)	21
2.6.2	Gradient Dependent Monitor Function	23
2.7	Application of Mass Balance Equation	25
2.8	Matrix Inversion	26
2.9	Results from Equidistribution Method for Planar Geometry .	28
2.9.1	Boundary Quadratic Velocity	29
2.9.2	Convergent Solution	31

3	1D Radial Case	34
3.1	Problem Construction	34
3.2	Mapping from Physical Grid to Logical Grid	36
3.3	Choice of Monitor Function	38
3.4	Application of Mass Balance Equation	41
3.5	Results and Conclusions From the Equidistribution Method for Radial Geometry	43
3.5.1	Large Solution Region - $J = 0.01Am^{-2}$	43
3.5.2	Change in Solution Region Size with Current Density .	45
3.5.3	Change in Solution Region Size with Accelerating Voltage	46
3.5.4	The Effect of the Parameter γ	47
4	Conclusions and Further Work	51
4.1	Conclusion	51
4.2	Further Work	53
4.2.1	Convergence	53
4.2.2	Stability	53

List of Figures

1.1	Neutron tube schematic	7
1.2	Schematic of 2D free boundary problem	8
2.1	1D Planar problem setup	10
2.2	Position of calculated free boundary	13
2.3	Change in potential across the solution region for varying emission current densities.	14
2.4	Change in solution region size with emission current density.	15
2.5	Change in solution potential with distance from fixed boundary for varying solution region potential differences.	16
2.6	Variation in free boundary position as a function of accelerating potential (constant current density and initial ion energy).	17
2.7	Change in solution potential with distance from the fixed boundary for varying accelerating potentials, and typical neutron tube current density.	18
2.8	Output from the equidistribution method at differing times for the conditions $J = 1Am^{-2}$, $\phi_0=0KV$, $\phi_n=100KV$ and an initial ion energy of 50eV	29
2.9	Distance of moving boundary from fixed boundary ($J = 1Am^{-2}$, $\phi_0=0KV$, $\phi_n=100KV$ and an initial ion energy of 50eV)	30

2.10 Output from the equidistribution method at differing times for the conditions for $J = 1Am^{-2}$, $\phi_0=0KV$, $\phi_n=100KV$ and an initial ion energy of 50eV. The RHS of the mass balance equation has been set to zero 31

2.11 Distance of moving boundary from fixed boundary ($J = 1Am^{-2}$, $\phi_0=0KV$, $\phi_n=100KV$ and an initial ion energy of 50eV). The RHS of the mass balance equation has been set to zero 32

2.12 Change in solution region size with emission current density (equidistribution method) 33

3.1 1D Radial problem setup 35

3.2 Analytic free boundary and radial moving boundary solutions for the conditions $J = 0.01Am^{-2}$ and $(\phi_n - \phi_0) = 100KV$ 44

3.3 Position of moving boundary as a function of time for the radial solution with conditions $J = 0.01Am^{-2}$ and $(\phi_n - \phi_0) = 100KV$ 45

3.4 Nodal position as a function of time for the condition $J = 0.01Am^{-2}$ and $(\phi_n - \phi_0) = 100KV$ 46

3.5 Nodal positions relative to their starting point as a function of time (for the condition $J = 0.01Am^{-2}$ and $(\phi_n - \phi_0) = 100KV$.) 47

3.6 Variation in potential across the solution region for different emission current densities. 48

3.7 Change in solution potential with distance for varying solution region potential differences. 49

3.8 The effect of γ on nodal movement. 50

Chapter 1

Introduction

The neutron generator group at AWE are primarily concerned with the design of a small particle accelerator called a *Neutron Tube*. These devices provide a short high intensity pulse of neutrons which are used in applications such as oil exploration and (of course) nuclear weapons.

1.1 Neutron Tube Basic Operation

In order to produce the pulse of neutrons, the neutron tube utilises the deuterium-tritium fusion reaction which has a peak cross section of $\sim 120\text{KeV}$. For the fusion reaction to take place, deuterium (or tritium) ions must be accelerated to an energy of $\sim 120\text{KeV}$ before striking a tritiated (or deuterated) target thereby releasing neutrons with 14.1MeV (in addition to 3.5MeV alpha particles).

To create the D-T reaction, the tube consists of an evacuated sealed envelope across which the acceleration voltage is held off. A source of deuterium ions is situated at one end of the tube (it is usual for deuterium ions to be accelerated onto a tritiated target rather than the converse) whilst the tritiated target is at the cathode end (see Figure 1.1) Upon operation, a plasma of deuterium ions expands into the acceleration gap forming a conductive 'gas' which is generally impenetrable to the tube main accelerating field (due

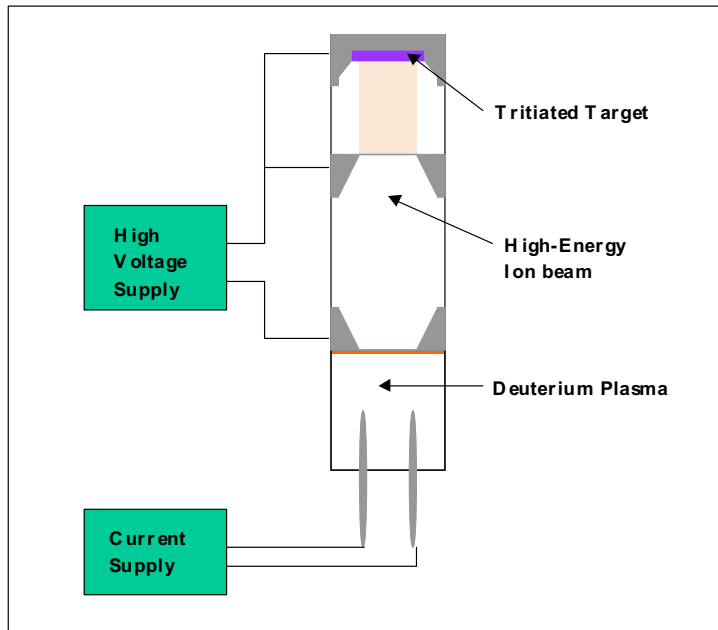


Figure 1.1: Neutron tube schematic

to this conductivity). At about the same time, the accelerating voltage is applied across the tube, and ions begin streaming away from the plasma-vacuum interface formed by the expanding plasma. Shaped electrodes within the tube act as ion lenses focussing the ion beam onto the tritiated target where the fusion reaction takes place.

Ions reaching the plasma-vacuum boundary at a specific rate cause the boundary to bulge into the vacuum, thereby concentrating the electric field within the region (since the plasma acts as a boundary for the electric field within the tube main gap). The increased electric field causes ions to be accelerated away from the boundary more rapidly than they arrive there, and consequently the boundary recedes until the electric field at the boundary is zero. In this final equilibrium state, ions leave the boundary at the same rate they arrive there.

The determination of the equilibrium position of the plasma-vacuum boundary, with a specific current density of ions arriving at the boundary,

and a specific potential difference across the main accelerating gap, is a free boundary problem.

1.2 Free Boundary Problem

The ultimate aim in solving this problem is to be able to predict the position of the plasma-vacuum boundary for two dimensional regions with geometrically complex boundaries and associated boundary conditions. A schematic of the problem in 2D is shown in Figure 1.2. Referring to Figure 1.2, either

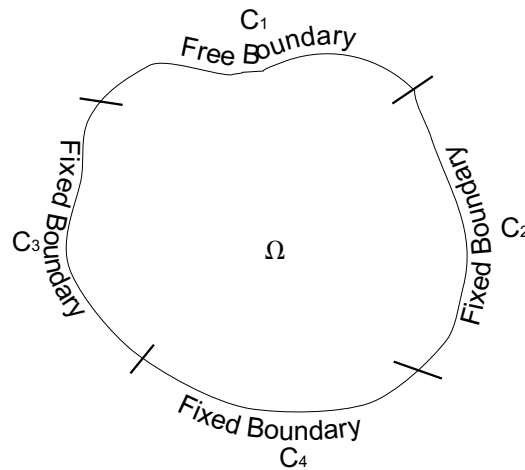


Figure 1.2: Schematic of 2D free boundary problem

Neumann or Dirichlet conditions are placed on each of the boundaries C_1 to C_4 , and C_1 has the added condition

$$\frac{\partial U}{\partial n} = 0$$

which is required to determine the boundary shape (n being normal to C_1), along with a specified current density. The governing equation describing the electrostatic potential within the region Ω is Poisson's equation, which in this instance in cartesian coordinates is given by

$$\nabla^2 U = \frac{-\rho(x, y)}{\epsilon_0} \quad (1.1)$$

Here $\rho(x, y)$ is a source term representing the free charge density within Ω , and ϵ_0 is a scale factor termed the permittivity of free space.

It is the purpose of this dissertation to solve a simplified 1D version of this free boundary problem for both radial and planar geometries.

1.3 Solution Approach

In Chapter 2 we begin with an essentially analytic solution to a reduced 1D planar version of (1.1) and explore the solutions generated.

Since the equivalent 1D radial problem cannot be solved in the same way, we modify the problem by introducing a pseudo-time variable and make the assumption that the solution of the now parabolic *moving boundary* problem tends to the solution of the original *free boundary* problem as time tends to infinity.

In order to solve the parabolic moving boundary problem, we introduce a numerical method based upon equidistribution of nodes (Section 2.3) in a logical space and apply it to the planar case.

Once confidence is established that the method works in the 1D planar case, we reformulate the method and apply it to the 1D radial case (Chapter 3), and again explore the solutions generated.

Chapter 2

1D Planar Case

The problem outlined in Section 1.2 can be reduced to the 1D planar problem shown in Figure 2.1. Within the region Ω , Poisson's equation (1.1) is

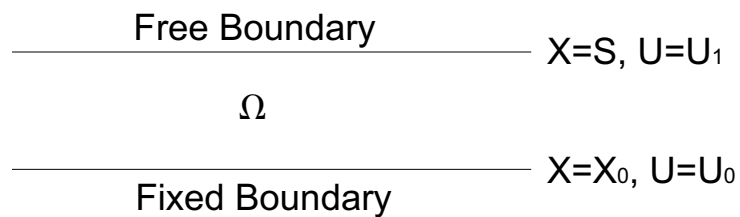


Figure 2.1: 1D Planar problem setup

reduced to the second order ODE

$$\frac{d^2U}{dx^2} = -\frac{\rho(x)}{\epsilon_0} \quad (2.1)$$

which is subject to the following boundary conditions

$$\left. \begin{array}{l} U = U_0, x = x_0 \\ U = U_1 \\ \frac{dU}{dx} = 0 \end{array} \right\} x = S \quad (2.2)$$

2.1 Analytic Solution

In order to solve (2.1) subject to (2.2), an expression relating the charge density $\rho(x)$ (at any point within Ω) to the solution potential and the current density at the free boundary is required. This relationship is found from the expression

$$\rho(x) = \frac{J}{v(x)}, \quad (2.3)$$

where $v(x)$ is the particle velocity at a position x within Ω . In this 1D case, the current density J at the free boundary is a constant. Clearly from (2.3) as the particle velocity increases (due to acceleration from a large electric field), particles spend less time within a unit volume thereby causing the charge density $\rho(x)$ to decrease.

The form of the particle velocity $v(x)$ is also required to integrate (2.1), and is found by equating the force exerted on a particle of charge q by the electric field within the region Ω , and the force required to accelerate a particle of specific mass m ,

$$\begin{aligned} F &= qE = -q \frac{dU}{dx} \\ &= mv(x) \frac{dv}{dx} \end{aligned} \quad (2.4)$$

Rewriting (2.4) as

$$\frac{m}{2} \frac{d}{dx} (v(x)^2) = -q \frac{dU}{dx}$$

allows immediate integration to give

$$v(x)^2 = -\frac{2q}{m}U(x) + c_1 \quad (2.5)$$

with c_1 being a constant of integration. When $x = S$, $U = U_1$ and $v(x) = v_0$ (the initial velocity of an emerging particle) such that

$$c_1 = v_0^2 + \frac{2q}{m}U_1$$

and

$$v(x) = \sqrt{\frac{2q}{m}(U_1 - U(x)) + v_0^2} \quad (2.6)$$

From (2.3) and (2.6) the ODE (2.1) becomes,

$$\frac{d^2U}{dx^2} = -\frac{J}{\epsilon_0} \left(\frac{2q}{m} (U_1 - U(x)) + v_0^2 \right)^{-\frac{1}{2}} \quad (2.7)$$

Multiplying (2.7) by $2\frac{dU}{dx}$ gives,

$$\frac{d}{dx} \left(\frac{dU}{dx} \right)^2 = -\frac{2J}{\epsilon_0} \left(\frac{2q}{m} (U_1 - U(x)) + v_0^2 \right)^{-\frac{1}{2}} \frac{dU}{dx}$$

which again allows immediate integration, giving

$$\left(\frac{dU}{dx} \right)^2 = \frac{2Jm}{q\epsilon_0} \left(\frac{2q}{m} (U_1 - U(x)) + v_0^2 \right)^{\frac{1}{2}} + c_2 \quad (2.8)$$

From (2.2), $\frac{dU}{dx} = 0$ when $U = U_1$ so that

$$c_2 = -\frac{2Jm}{q\epsilon_0} v_0$$

and

$$\frac{dU}{dx} = \sqrt{\frac{2Jm}{q\epsilon_0} \left\{ \left(\frac{2q}{m} (U_1 - U(x)) + v_0^2 \right)^{\frac{1}{2}} - v_0 \right\}} \quad (2.9)$$

The integration of (2.9) is not possible analytically, and so we appeal to a standard explicit fourth order Runge-Kutta method to perform the integration.

2.2 Results from Analytic Solution

The forward stepping R-K algorithm is executed until the calculated solution derivative $\frac{dU}{dx}$ at each step falls below a tolerance. Since the discrete spatial steps are constant in size, it is usual that the calculated derivative at the penultimate node will fall outside the tolerance, such that a final step must be taken. The constant step size will in general not be equal to the

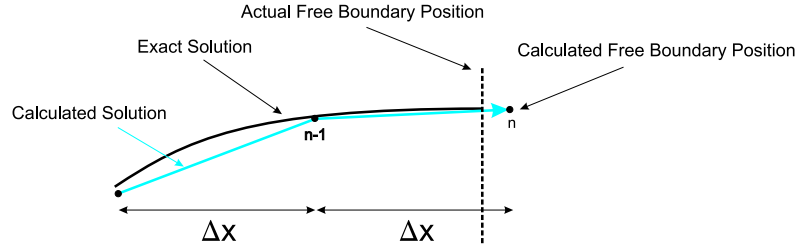


Figure 2.2: Position of calculated free boundary

distance between the penultimate node and the actual free boundary position. The final node is then beyond the free boundary causing the RHS of (2.9) to be undefined. This error condition is trapped, and the calculated free boundary position is given as the position of this final node (see Figure 2.2).

The integration of (2.9) has been performed for a number of different initial conditions in order to test the solution against expected results. In all studies of the planar solution, the particle mass and charge are those of a deuteron, and quantities that are varied are the initial particle velocity v_0 , the current density at the free boundary J , and the accelerating potential difference ($U_1 - U_0$).

It is expected that as J increases, plasma will bulge into the solution region Ω such that the free boundary will settle closer to the fixed boundary (at its equilibrium position), for a fixed potential difference. Similarly, if the accelerating potential difference is small, plasma will again bulge into Ω such that the free boundary settles (relatively) close to the fixed boundary. This expected behaviour is examined.

In addition to examination of the above behaviour, parameters relating to a typical neutron tube (the mean current density, initial particle velocity for a 50eV deuteron, and main gap accelerating voltage) are used to find the position of the free boundary in this case. It is expected that the calculated main gap dimensions will be of a similar order of magnitude to those of

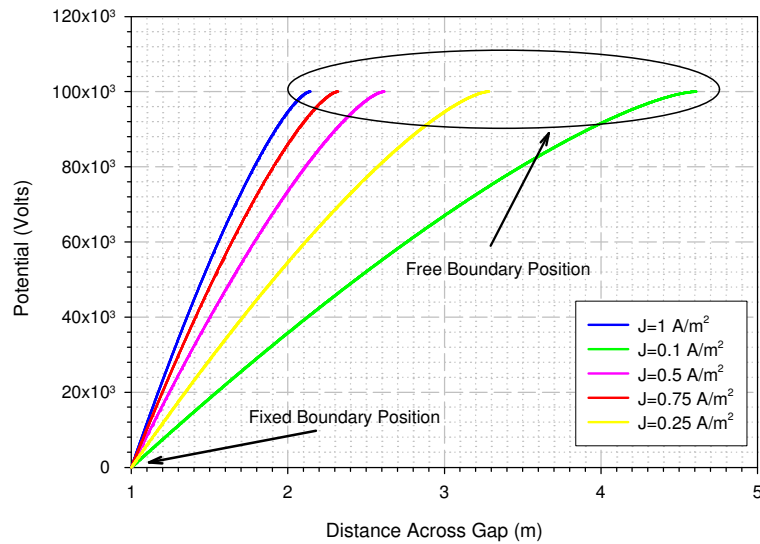


Figure 2.3: Change in potential across the solution region for varying emission current densities.

typical neutron tube that has been designed to operate below space charge limitation.

2.2.1 Variation in Solution Region Size with Emission Current Density

As mentioned above, it is expected that as the current density increases with a constant accelerating voltage (and constant emerging particle energy), the distance between the free and fixed boundary will reduce accordingly. Figure 2.3 clearly shows this for an accelerating voltage of 100KV, and a variation in current density from 0.1A/m^{-2} to 1.0A/m^{-2} .

Referring to Figure 2.3, as the current density increases, the plasma bulges into the solution region thereby reducing the gap between the free and fixed boundaries. This is more clearly shown in Figure 2.4.

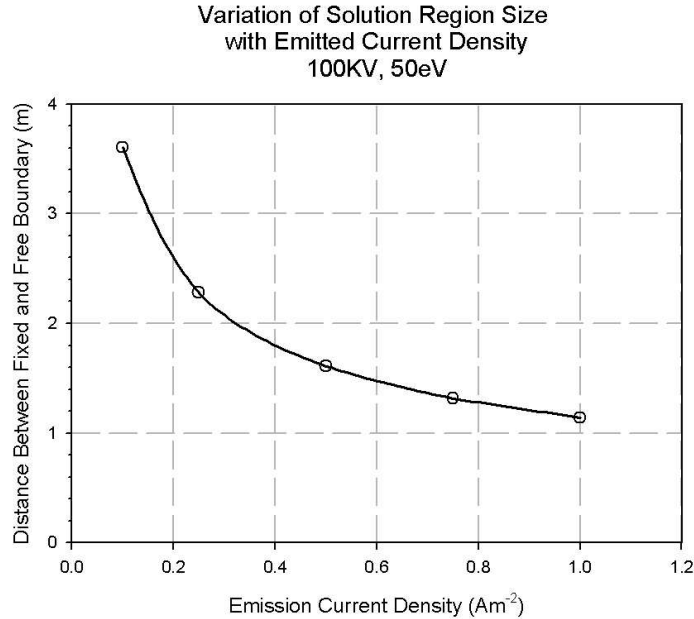


Figure 2.4: Change in solution region size with emission current density.

2.2.2 Variation in Solution Region Size with Accelerating Potential

Again as previously mentioned, it is expected that as the potential difference across the solution region increases, plasma is stripped off more readily from the free boundary emission region thereby causing the boundary to recede.

Figure 2.5 shows the calculated potential solution across the solution region for three different potential differences (with constant current density and constant initial ion energy). Examining the position of the point where the electric field (potential gradient) is zero (this is one of the boundary conditions defining the position of the free boundary), clearly indicates that the free boundary recedes away from the fixed boundary as the potential difference across the solution region increases. This is more clearly shown in Figure 2.6 where the free-fixed boundary distance is calculated as a function of accelerating potential.

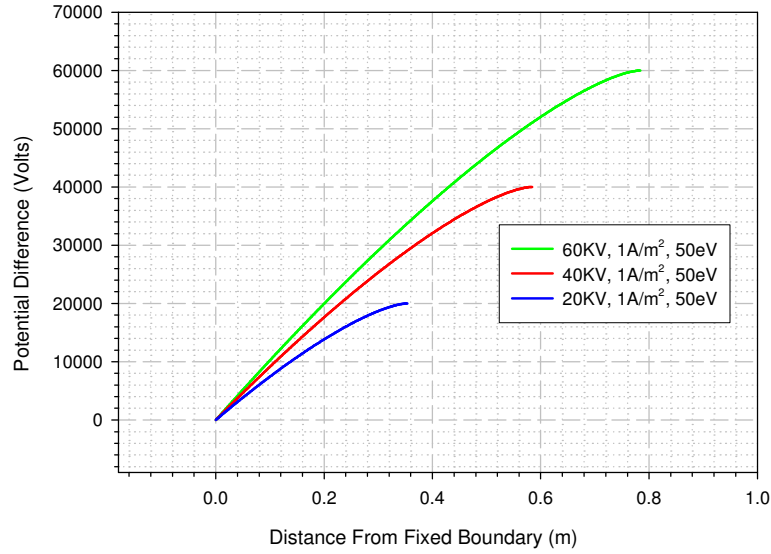


Figure 2.5: Change in solution potential with distance from fixed boundary for varying solution region potential differences.

2.2.3 Predicted Solution Region Size for a Typical Neutron Tube

The source current density for operation of a typical neutron tube was determined and used, along with a range of typical accelerating voltages, as input parameters to the planar calculation. The emitted ion energy was chosen to be 50eV (a generally accepted energy for ions leaving a deuterium plasma).

The neutron tube generally operates outside space charge limited conditions ¹. However, space charge limitation can be relatively easily achieved by lowering the tube accelerating voltage, or by significantly increasing the ion current density from the source. As such, the tube inter-electrode gap should be of a similar order of magnitude to the calculated free boundary to fixed boundary spacing (the gap that would exist in true space charge limited flow).

¹Space charge limitation is the equilibrium state where the flux of ions reaching the plasma boundary is equal to the flux of ions leaving it.

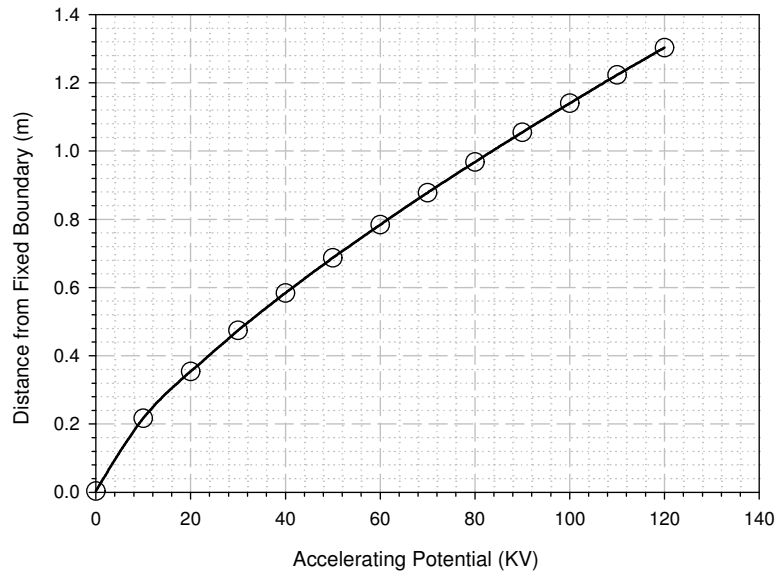


Figure 2.6: Variation in free boundary position as a function of accelerating potential (constant current density and initial ion energy).

Figure 2.7 shows the calculated solution for the planar free boundary problem with typical neutron tube operating parameters. Clearly, at 100KV, the calculated width of solution region is $\sim 8.5\text{mm}$ in comparison to the neutron tube inter-electrode gap² which is measured in mm . Although the free boundary calculation is not fully representative of the tube geometry due to being a planar calculation in 1D, the calculated distance between free and fixed boundary is similar indicating that the calculated solution is at least of the correct order of magnitude.

2.3 Equidistribution Method

The solution given in Section 2.1 is relatively easy to find, is for the main part analytical, and behaves exactly as expected. In order to find the equivalent solution in a radial coordinate system, we must appeal to a purely numeri-

²Accurate dimensions cannot be listed here.

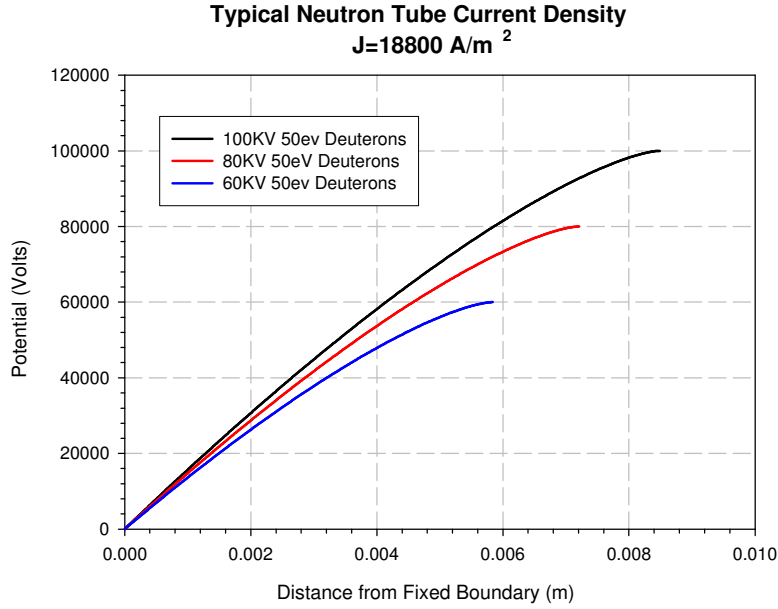


Figure 2.7: Change in solution potential with distance from the fixed boundary for varying accelerating potentials, and typical neutron tube current density.

cal method since a similar analysis to the planar case is not possible. The particular method used is a nodal equidistribution based method.

As an introduction, this method is initially applied to the planar case but the following analysis can also be applied to the radial problem as is shown in Chapter 3.

2.4 Introduction of Pseudo Time

In order to solve (2.7) subject to the conditions (2.2) using an iterative method, we introduce a pseudo time variable τ and rewrite (2.7) as a parabolic equation of the form

$$\frac{\partial \phi}{\partial \tau} = \frac{\partial^2 \phi}{\partial x^2} + g(\phi) \quad (2.10)$$

where $g(\phi)$ is the negative value of the RHS of (2.7) and the steady state

function $U(x)$ is now written as the time dependent function $\phi(x, \tau)$. An assumption is made that as $\tau \rightarrow \infty$, the function $\phi(x, \tau)$ converges to the steady state solution $U(x)$ (i.e. as $\tau \rightarrow \infty$, $\phi_\tau \rightarrow 0$ such that the original equation (2.7) holds) ³.

2.5 Mapping from Physical Grid to Logical Grid

The equation (2.10) subject to the boundary conditions (2.2) is now a moving boundary problem since the solution region evolves with the time variable τ . We therefore seek a time-stepping procedure that calculates the velocity of nodes within a discretised version of the physical solution region Ω (including the node at the moving boundary). Nodal positions may then be updated at each time-step along with the solution $\phi(x, \tau)$, and the procedure continued until the mean nodal velocity falls below a tolerance.

Mapping the nodes in the physical region Ω on to a logical region Ξ (the mapping must be both injective ⁴ and surjective ⁵) such that the distribution of nodes in the logical region is constant in time (the nodes in the logical region are equally spaced), allows the nodal velocities in the physical region to be calculated.

A mapping (or monitor) function M can be chosen such that

$$M \frac{dx}{d\xi} = 1 \quad (2.11)$$

where ξ represents the coordinate in the logical region Ξ . In this way, the rate of change of logical space variable ξ with physical space variable x is governed by the function M .

³The criteria for this to hold are not investigated here.

⁴Injective means that one node in the logical space maps to one node in the physical space.

⁵Surjective means that for every point in the logical space, there exists a point in the physical space.

Integration over the entire region Ω (and corresponding logical region Ξ) gives

$$\begin{aligned} \int_{x_0}^{x_n(\tau)} M dx &= \int_{\xi_0}^{\xi_n(\tau)} d\xi \\ &= \xi_n(\tau) - \xi_0 \\ &= \Theta(\tau). \end{aligned} \quad (2.12)$$

Here $x_n(\tau)$ corresponds to the moving outer boundary (S in Figure 2.1) indicating that Ω has been discretised with n nodal points. Integrating (2.11) over a single 'element' in the physical domain gives

$$\begin{aligned} \int_{x_{i-1}}^{x_i} M dx &= \int_{\xi_{i-1}}^{\xi_i} d\xi \\ &= \Delta\xi \end{aligned} \quad (2.13)$$

If the ratio, $\Delta\xi/(\xi_n(\tau) - \xi_0)$ is constant in time, then nodes in the logical region Ξ will be equally distributed indicating that

$$\frac{1}{\Theta(\tau)} \int_{x_{i-1}}^{x_i} M dx = c_{i-\frac{1}{2}} \quad (2.14)$$

where $c_{i-\frac{1}{2}}$ is a constant in time and refers to the i^{th} 'element'. Taking the derivative of (2.14) with respect to time gives

$$\frac{dc}{d\tau} = 0 = \frac{\partial c}{\partial x} \frac{dx}{d\tau} + \frac{\partial c}{\partial \tau} \quad (2.15)$$

($c_{i-\frac{1}{2}}$ is written c for brevity).

From (2.14), the first term on the RHS of (2.15) is given by

$$\frac{\partial c}{\partial x} \frac{dx}{d\tau} = \frac{1}{\Theta} \left[M \dot{x} \right]_{x_{i-1}}^{x_i} \quad (2.16)$$

and the second term on the RHS of (2.15) may be written

$$\frac{\partial c}{\partial \tau} = \int_{x_{i-1}}^{x_i} \frac{\partial}{\partial \tau} \left(\frac{M}{\Theta} \right) dx = 0, \quad (2.17)$$

which on expansion gives

$$\frac{\partial c}{\partial \tau} = \frac{1}{\Theta} \int_{x_{i-1}}^{x_i} \frac{\partial M}{\partial \tau} dx - \frac{\dot{\Theta}}{\Theta^2} \int_{x_{i-1}}^{x_i} M dx \quad (2.18)$$

Combining (2.16) and (2.18) such that

$$\int_{x_{i-1}}^{x_i} \frac{\partial M}{\partial \tau} dx - \frac{\dot{\Theta}}{\Theta} \int_{x_{i-1}}^{x_i} M dx + \left[M \dot{x} \right]_{x_{i-1}}^{x_i} = 0 \quad (2.19)$$

and approximating the integrals using the trapezium rule yields an $(n+1) \times n$ system of equations for the n nodal velocities and $\dot{\Theta}$ ($\dot{x}_0 = 0$).

Since this is not a square system, an additional equation is required, and this can be obtained from the mass balance equation,

$$\frac{d}{d\tau} \int_{x_0}^{x_n} \phi dx = \int_{x_0}^{x_n} \frac{\partial^2 \phi}{\partial x^2} + g(\phi) dx \quad (2.20)$$

relating to the DE (2.10).

2.6 Choice of Monitor Function

2.6.1 Equally Distributed Nodes ($M = 1$)

Initially choosing the monitor function M to be equal to 1 means that from (2.11) nodes in the physical domain are equally spaced, since the rate of change of physical coordinate with logical coordinate is 1. From (2.12) and (2.13), the ratio $\Delta\xi/(\xi_n(\tau) - \xi_0)$ is given by

$$\begin{aligned} \frac{\Delta\xi}{\xi_n(\tau) - \xi_0} &= \frac{x_i - x_{i-1}}{x_n - x_0} \\ &= c_{i-\frac{1}{2}} \end{aligned} \quad (2.21)$$

which again clearly indicates that nodes in the physical domain are equally distributed. As time progresses, if the moving boundary at $x_n(\tau)$ moves in a positive x direction then in order for the ratio (2.21) to remain constant

in time, the node at x_i will have a slightly higher velocity than the node at x_{i-1} such that the i^{th} element increases in size accordingly (e.g for the first 'element' x_0 is fixed, and x_1 must move in a positive x direction to ensure that the ratio is held constant).

Referring then to (2.19), the system of equations relating the nodal velocities \dot{x} and $\dot{\Theta}$ is given by

$$[\dot{x}]_{x_{i-1}}^{x_i} - \frac{\dot{\Theta}}{\Theta} \int_{x_{i-1}}^{x_i} dx = 0,$$

which for the i^{th} equation is

$$\dot{x}_i - \dot{x}_{i-1} - c_{i-\frac{1}{2}} \dot{\Theta} = 0 \quad (2.22)$$

Referring to the mass balance equation (2.20), the LHS can be re-written

$$\frac{d}{d\tau} \int_{x_0}^{x_n} \phi dx = \frac{\partial}{\partial \tau} \int_{x_0}^{x_n} \phi dx + [\phi \dot{x}]_{x_0}^{x_n} \quad (2.23)$$

and approximating the integral on the RHS of (2.23) using the trapezium rule gives

$$\begin{aligned} \frac{\partial}{\partial \tau} \int_{x_0}^{x_n} \phi dx &\approx \frac{\partial}{\partial \tau} \left(\frac{1}{2} \sum_{i=1}^n (x_i - x_{i-1}) (\phi_i + \phi_{i-1}) \right) \\ &\approx \frac{1}{2} \sum_{i=1}^n (\phi_i + \phi_{i-1}) (\dot{x}_i - \dot{x}_{i-1}) + \dots \\ &\dots + (x_i - x_{i-1}) (\dot{\phi}_i + \dot{\phi}_{i-1}) \end{aligned} \quad (2.24)$$

with the second term on the RHS of (2.23) being given by

$$[\phi \dot{x}]_{x_0}^{x_n} = \phi_n \dot{x}_n \quad (2.25)$$

since $\dot{x}_0 = 0$. The RHS of the mass balance equation (2.20) can also be re-written with the first term being given by

$$\int_{x_0}^{x_n(\tau)} \frac{\partial^2 \phi}{\partial x^2} dx = - \left. \frac{\partial \phi}{\partial x} \right|_{x_0}, \quad (2.26)$$

since $\frac{\partial \phi}{\partial x} = 0$ (from the BCs (2.2)). The second term can then be approximated

$$\int_{x_0}^{x_n(\tau)} g(\phi) dx \approx \frac{1}{2} \sum_{i=1}^n (x_i - x_{i-1}) (g(\phi_i) + g(\phi_{i-1})) \quad (2.27)$$

Combining (2.24), (2.25), (2.26), and (2.27) gives an expression relating the nodal velocities $\underline{\dot{x}}$ and the nodal rate of change of solution $\dot{\phi}$,

$$\begin{aligned} \frac{1}{2} \sum_{i=1}^{n-1} (\phi_{i-1} - \phi_{i+1}) \dot{x}_i + \frac{1}{2} (3\phi_n + \phi_{n-1}) \dot{x}_n + \frac{1}{2} \sum_{i=1}^{n-1} (x_{i+1} - x_{i-1}) \dot{\phi}_i = \\ - \left. \frac{\partial \phi}{\partial x} \right|_{x_0} + \frac{1}{2} \sum_{i=1}^{n-1} (x_{i+1} - x_{i-1}) g(\phi_i) + \dots \\ \dots + \frac{(x_1 - x_0)}{2} g(\phi_0) + \frac{(x_n - x_{n-1})}{2} g(\phi_n) \end{aligned} \quad (2.28)$$

Due to the choice of monitor function, there is no apparent way of linking the nodal velocities $\underline{\dot{x}}$ and $\dot{\Theta}$ from equation (2.28). In addition, the differential equation (2.10) does not appear globally in the system (2.22). As such it is deemed that the use of the monitor function $M = 1$ in this application is fruitless. We therefore seek a different monitor function which enables a relationship between $\underline{\dot{x}}$ and $\dot{\Theta}$ to be established from the mass balance equation, and one which allows the differential equation under study to be more globally applied throughout the \dot{x} equations.

2.6.2 Gradient Dependent Monitor Function

If we choose $M = 1 + \gamma \phi_x$ (γ being a constant) then from (2.11) it is clear that when the solution gradient ϕ_x is large, the rate of change of nodes in the physical domain with respect to the logical domain is small (i.e. nodes are concentrated around areas where the solution changes rapidly). As in section 2.6.1, from (2.12) and (2.13) the ratio $\Delta\xi / (\xi_n(\tau) - \xi_0)$ is now given by

$$\begin{aligned} \frac{\Delta\xi}{\xi_n(\tau) - \xi_0} &= \frac{(x_i - x_{i-1}) + \gamma(\phi_i - \phi_{i-1})}{(x_n - x_0) + \gamma(\phi_n - \phi_0)} \\ &= c_{i-\frac{1}{2}} \end{aligned} \quad (2.29)$$

If the moving boundary moves in a positive x direction, the denominator of the term on the RHS of (2.29) will increase. In order that this term remain constant in time, either the solution gradient within the i^{th} 'element'

$(\phi_i - \phi_{i-1})$ must increase, the width of the element must increase $(x_i - x_{i-1})$, or a combination of both. If the solution gradient within the i^{th} element is large relative to the element size, then the element width will not have to increase greatly to ensure that (2.29) remains constant (indicating that nodal velocities in areas of steep solution gradient should be small).

Following a similar analysis to section 2.6.1 and substituting $M = 1 + \gamma\phi_x$ into the expression (2.19) yields

$$\gamma \int_{x_{i-1}}^{x_i} \phi_{x\tau} dx - c_{i-\frac{1}{2}} \dot{\Theta} + \left[(1 + \gamma\phi_x) \dot{x} \right]_{x_{i-1}}^{x_i} = 0 \quad (2.30)$$

which again represents an $(n + 1) \times n$ system of equations for the nodal velocities \dot{x} and $\dot{\Theta}$. The first term on the LHS of (2.30) can be written

$$\begin{aligned} \gamma \int_{x_{i-1}}^{x_i} \phi_{x\tau} dx &= \gamma [\phi_\tau]_{x_{i-1}}^{x_i} \\ &= \gamma \left[\phi_{xx} + g(\phi) \right]_{x_{i-1}}^{x_i} \end{aligned} \quad (2.31)$$

from the original equation (2.10), and the RHS of (2.31) can be approximated using differences:

When $i = 1$,

$$\begin{aligned} \gamma \left[\phi_{xx} + g(\phi) \right]_{x_{i-1}}^{x_i} &\approx \gamma \left\{ \left(\frac{\frac{\partial\phi}{\partial x}|_{x_2} - \frac{\partial\phi}{\partial x}|_{x_0}}{(x_2 - x_0)} \right) - \dots \right. \\ &\quad \left. \dots - \left(\frac{\frac{\partial\phi}{\partial x}|_{x_1} - \frac{\partial\phi}{\partial x}|_{x_0}}{(x_1 - x_0)} \right) + g(\phi_1) - g(\phi_0) \right\} \\ &= -b_1 \end{aligned} \quad (2.32)$$

using central and backward differences to approximate $\phi_{xx}|_1$ and $\phi_{xx}|_0$ respectively.

When $i = 2$ to $n - 1$,

$$\gamma \left[\phi_{xx} + g(\phi) \right]_{x_{i-1}}^{x_i} \approx \gamma \left\{ \left(\frac{\frac{\partial\phi}{\partial x}|_{x_{i+1}} - \frac{\partial\phi}{\partial x}|_{x_{i-1}}}{(x_{i+1} - x_{i-1})} \right) - \dots \right.$$

$$\begin{aligned} \dots & - \left(\frac{\frac{\partial\phi}{\partial x}|_{x_i} - \frac{\partial\phi}{\partial x}|_{x_{i-2}}}{(x_i - x_{i-2})} + g(\phi_i) - g(\phi_{i-1}) \right) \\ & = -b_i \end{aligned} \quad (2.33)$$

using central differences to approximate both $\phi_{xx}|_i$ and $\phi_{xx}|_{i-1}$.

When $i = n$,

$$\begin{aligned} \gamma \left[\phi_{xx} + g(\phi) \right]_{x_{n-1}}^{x_n} & \approx \gamma \left\{ \left(\frac{-\frac{\partial\phi}{\partial x}|_{x_{n-1}}}{(x_n - x_{n-1})} - \dots \right. \right. \\ & \dots - \left. \left(\frac{-\frac{\partial\phi}{\partial x}|_{x_{n-2}}}{(x_n - x_{n-2})} + g(\phi_n) - g(\phi_{n-1}) \right) \right\} \\ & = -b_n \end{aligned} \quad (2.34)$$

using backward and central differences to approximate $\phi_{xx}|_n$ and $\phi_{xx}|_{x_{n-1}}$ respectively (and since $\frac{\partial\phi}{\partial x}|_{x_n} = 0$).

The system of equations (2.30) can then be written

$$\begin{aligned} & \begin{pmatrix} \left(1 + \gamma \frac{\partial\phi}{\partial x}\right)|_{x_1} & 0 & 0 & \dots & -c_{\frac{1}{2}} \\ -\left(1 + \gamma \frac{\partial\phi}{\partial x}\right)|_{x_1} & \left(1 + \gamma \frac{\partial\phi}{\partial x}\right)|_{x_2} & 0 & & -c_{\frac{3}{2}} \\ \vdots & \ddots & \ddots & & \vdots \\ 0 & & -\left(1 + \gamma \frac{\partial\phi}{\partial x}\right)|_{x_{n-1}} & 1 & -c_{n-\frac{1}{2}} \end{pmatrix} \times \dots \\ & \dots \times \begin{pmatrix} \dot{x}_1 \\ \dot{x}_2 \\ \vdots \\ \dot{x}_n \\ \dot{\Theta} \end{pmatrix} = \begin{pmatrix} b_1 \\ b_2 \\ \vdots \\ b_n \end{pmatrix} \end{aligned} \quad (2.35)$$

2.7 Application of Mass Balance Equation

Since this system is not square, the discretised mass balance equation (2.28) is required to offer an additional relationship between the nodal velocities $\underline{\dot{x}}$

and $\dot{\Theta}$. In order to use (2.28) an expression relating $\dot{\Theta}$ and $\dot{\phi}_i$ must be found. Referring to (2.29) and summing the constants $c_{i-\frac{1}{2}}$ from $i+1$ to n gives

$$\sum_{j=i+1}^n c_{j-\frac{1}{2}} = \frac{\gamma(\phi_n - \phi_i) + (x_n - x_i)}{\Theta} \quad (2.36)$$

(using the expression (2.12) for theta in the denominator of (2.29)). Rearrangement of (2.36) gives an expression for ϕ_i in terms of Θ ,

$$\phi_i = \phi_n - \frac{\Theta \overline{C}_i}{\gamma} + \frac{1}{\gamma}(x_n - x_i) \quad (2.37)$$

where the summation in (2.36) is replaced by \overline{C}_i for brevity. Taking the time derivative of this gives us the required relationship

$$\dot{\phi}_i = -\frac{\dot{\Theta} \overline{C}_i}{\gamma} + \frac{1}{\gamma}(\dot{x}_n - \dot{x}_i), \quad (2.38)$$

which can now be substituted into (2.28). Performing the substitution and collecting terms gives the required final equation in \dot{x} and $\dot{\Theta}$,

$$\begin{aligned} & \frac{1}{2} \left(\sum_{i=1}^{n-1} \left\{ (\phi_{i-1} - \phi_{i+1}) - \frac{1}{\gamma}(x_{i+1} - x_{i-1}) \right\} \right) \dot{x}_i + \frac{1}{2} \left((3\phi_n + \phi_{n-1}) + \dots \right. \\ & \quad \left. \dots + \frac{1}{\gamma} \sum_{i=1}^{n-1} (x_{i+1} - x_{i-1}) \right) \dot{x}_n - \frac{1}{2\gamma} \left(\sum_{i=1}^{n-1} \overline{C}_i (x_{i+1} - x_{i-1}) \right) \dot{\Theta} \\ & = \left. \frac{\partial \phi}{\partial x} \right|_{x_0} + \frac{1}{2} \sum_{i=1}^{n-1} (x_{i+1} - x_{i-1}) g(\phi_i) + \frac{(x_1 - x_0)}{2} g(\phi_0) + \dots \\ & \quad \dots + \frac{(x_n - x_{n-1})}{2} g(\phi_n) \quad (2.39) \end{aligned}$$

Adding the line (2.39) to (2.35) gives a square system for \dot{x} and $\dot{\Theta}$ with a characteristic bi-banded structure.

2.8 Matrix Inversion

The system generated from (2.35) and (2.39) can be represented by

$$\mathbf{A} \begin{pmatrix} \dot{x} \\ \dot{\Theta} \end{pmatrix} = \underline{b} \quad (2.40)$$

where

$$\mathbf{A} = \begin{pmatrix} \mathbf{B} & \underline{c}_1 \\ \underline{R} & s \end{pmatrix}, \quad \underline{b} = \begin{pmatrix} \underline{b}_1 \\ e \end{pmatrix}. \quad (2.41)$$

and

\mathbf{B} is an $n \times n$ bi-diagonal matrix (columns 1 to n in (2.35)),

\underline{c}_1 is a column vector of length n (column $n + 1$ in (2.35)),

\underline{R} is a row vector of length n (given by the \dot{x}_i and \dot{x}_n coefficients in (2.39)),

s is a scalar (given by the $\dot{\Theta}$ coefficient in (2.39)),

\underline{b}_1 is a column vector of length n (given by the RHS of (2.35)),

e is a scalar (given by the RHS of (2.39)).

It is noted that due to the structure of the bi-diagonal matrix \mathbf{A} shown in (2.35), addition of successive rows will cancel the off-diagonal elements rendering the matrix diagonal. Therefore adding successive rows of \mathbf{A} and \underline{b} from 1 to n we have,

$$\mathbf{M} \begin{pmatrix} \dot{x} \\ \dot{\Theta} \end{pmatrix} = \underline{n} \quad (2.42)$$

where

$$\mathbf{M} = \begin{pmatrix} \mathbf{D} & \underline{c}_2 \\ \underline{R} & s \end{pmatrix}, \quad \underline{b} = \begin{pmatrix} \underline{b}_2 \\ e \end{pmatrix}. \quad (2.43)$$

Now

\mathbf{D} is an $n \times n$ diagonal matrix,

\underline{c}_2 is a column vector of length n (formed by the addition of successive rows of \underline{c}_1),

\underline{b}_2 is a column vector of length n (formed by the addition of successive rows of \underline{b}_1).

Multiplying out the first row of (2.42) gives

$$\mathbf{D}\dot{x} + \underline{c}_2\dot{\Theta} = \underline{b}_2 \quad (2.44)$$

such that

$$\dot{x} = \mathbf{D}^{-1}(\underline{b}_2 - \underline{c}_2\dot{\Theta}) \quad (2.45)$$

Also from (2.42),

$$\underline{R}\dot{x} + s\dot{\Theta} = e \quad (2.46)$$

Substituting \dot{x} from (2.45) into (2.46)

$$\underline{R}\mathbf{D}^{-1}(\underline{b}_2 - \underline{c}_2\dot{\Theta}) + s\dot{\Theta} = e \quad (2.47)$$

and rearranging gives,

$$\dot{\Theta} = \left(e - \underline{R}\mathbf{D}^{-1}\underline{b}_2 \right) \cdot \frac{1}{\underline{R}\mathbf{D}^{-1}(-\underline{c}_2) + s} \quad (2.48)$$

Once $\dot{\Theta}$ has been calculated from (2.48), substitution into (2.45) will give the vector \dot{x} .

2.9 Results from Equidistribution Method for Planar Geometry

The iterative method of solution provided by the equidistribution method proceeds in the following way:

An initial solution region width is arbitrarily chosen, and an initial solution condition generated across this region (in this case the initial solution condition was chosen to be a straight line stretching across the region and ranging in height from ϕ_0 to ϕ_n).

A time-stepping loop is started and the system of equations generated from (2.35) and (2.39) is constructed. The solution of this system is found from (2.48) and then (2.45). Since the nodal velocities \dot{x}_i have been found, the nodal positions for the next time step are updated along with the value

of Θ (found from (2.12)). The solution at the nodes ϕ_i is now found from (2.37).

This procedure is repeated until the RMS nodal velocity falls below a tolerance (or until the procedure is called to stop).

2.9.1 Boundary Quadratic Velocity

Initially the procedure was applied to a specific condition used for the analytic method in Section 2.1 ($J = 1Am^{-2}$, $\phi_0=0KV$, $\phi_n=100KV$ and an initial ion energy of 50eV). It was expected that as time progressed, the solution would move away from the initial condition and slowly converge towards the analytic solution. However, Figure 2.8 shows the results of the method where it is clear that convergence is not taking place.

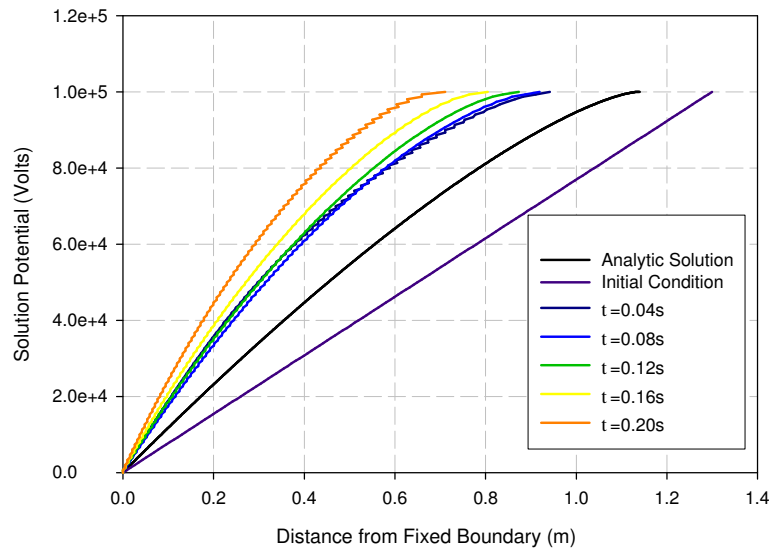


Figure 2.8: Output from the equidistribution method at differing times for the conditions $J = 1Am^{-2}$, $\phi_0=0KV$, $\phi_n=100KV$ and an initial ion energy of 50eV

Furthermore, the moving boundary appears to be moving with an almost parabolic velocity as is apparent in Figure 2.9. The cause of this

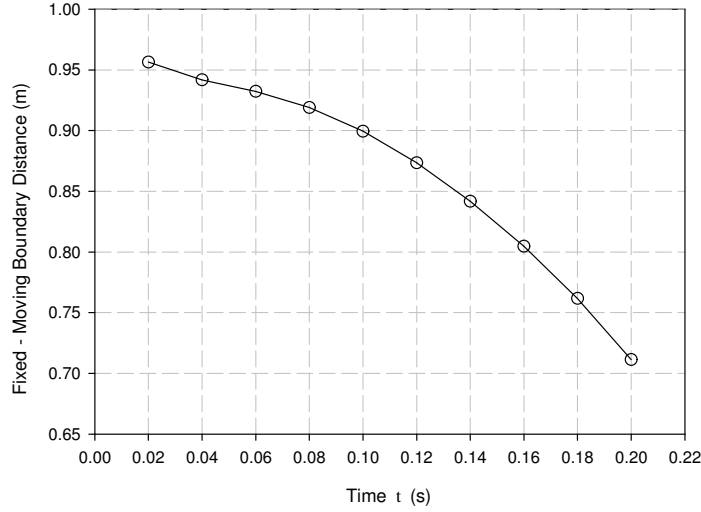


Figure 2.9: Distance of moving boundary from fixed boundary ($J = 1Am^{-2}$, $\phi_0=0KV$, $\phi_n=100KV$ and an initial ion energy of 50eV)

non-convergence comes from the application of time to an originally time independent problem (which is highly nonlinear and has the boundary velocity implicitly defined). Integration of the original differential equation (2.1) on the RHS of the mass balance equation (2.20) will give rise to an arbitrary constant

$$\int_{x_0}^{x_n} \frac{\partial^2 \phi}{\partial x^2} + g(\phi) dx = k_1, \quad (2.49)$$

since the integrand is equal to zero (from the original DE (2.1)). Equating this to the LHS of the mass balance equation implies that the solution 'mass'⁶ has linear time dependence

$$\begin{aligned} \frac{d}{d\tau} \int_{x_0}^{x_n} \phi dx &= k_1 \\ \text{or, } \int_{x_0}^{x_n} \phi dx &= k_1 \tau + k_2 \end{aligned} \quad (2.50)$$

Since the height of the solution curve is fixed by the boundary conditions

⁶The area under the solution curve.

(2.2) and the solution is approximately linear (this is clear from Figure 2.5 amongst others), then in order for the solution 'mass' to have a linear time dependence, the solution region must change size quadratically as is roughly the case in Figure 2.9.

2.9.2 Convergent Solution

This problem is corrected by setting the RHS of the mass balance equation to be zero, thereby fixing the solution 'mass' in time and forcing the iterative method to converge. Setting the RHS of (2.39) to be zero in the iteration has the desired effect as is shown in Figure 2.10. Here the the same conditions as for Figure 2.8 were applied. Referring to Figure 2.10, the straight line initial

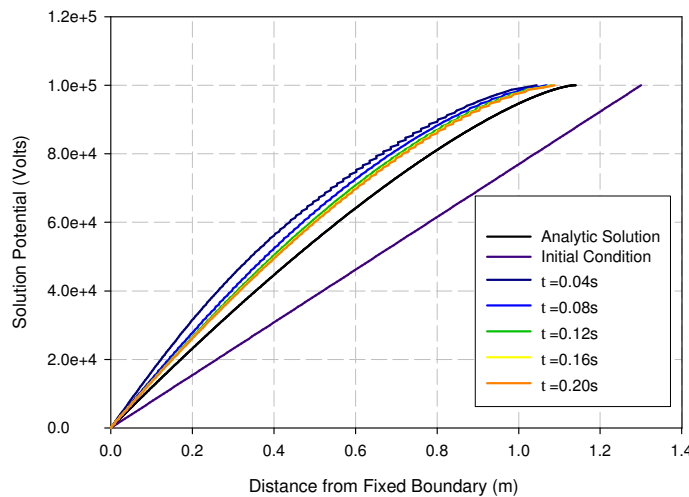


Figure 2.10: Output from the equidistribution method at differing times for the conditions for $J = 1Am^{-2}$, $\phi_0=0KV$, $\phi_n=100KV$ and an initial ion energy of 50eV. The RHS of the mass balance equation has been set to zero

condition is seen in addition to the analytic solution. As time progresses, the calculated solution curves are approaching the analytic solution. Figure 2.11 shows the position of the moving boundary, which is clearly approaching a limit as time progresses. Figure 2.12 is a repeat of Figure 2.3 but with the

solutions having been generated using the equidistribution method. Clearly the solution is behaving as expected since as the emission current density increases, the solution region reduces in size (see Section 2.2.1).

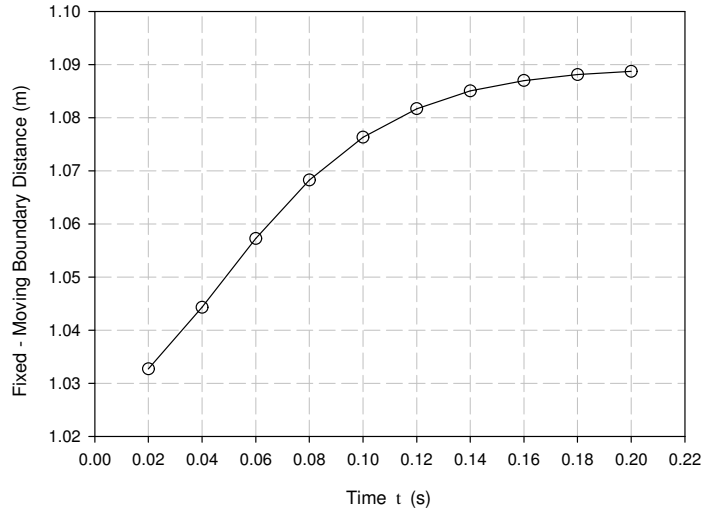


Figure 2.11: Distance of moving boundary from fixed boundary ($J = 1Am^{-2}$, $\phi_0=0KV$, $\phi_n=100KV$ and an initial ion energy of 50eV). The RHS of the mass balance equation has been set to zero

Now that the equidistribution method has been established, we use it to seek an equivalent solution in a radial coordinate system.

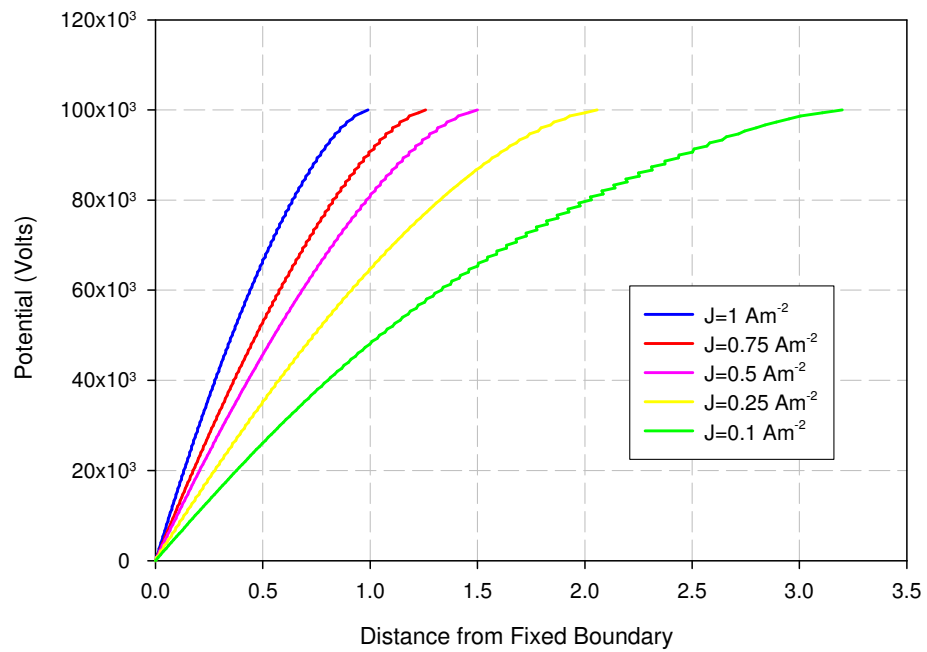


Figure 2.12: Change in solution region size with emission current density (equidistribution method)

Chapter 3

1D Radial Case

In order to construct a problem equivalent to that in Section 2 but in radial geometry, the original Poisson's equation (1.1) must be transformed into radial coordinates as follows,

$$\nabla^2 U(x, y) \rightarrow \frac{1}{r^2} \frac{\partial^2 \psi(r, \theta)}{\partial \theta^2} + \frac{\partial^2 \psi(r, \theta)}{\partial r^2} + \frac{1}{r} \frac{\partial \psi(r, \theta)}{\partial r} = -\frac{\rho(r, \theta)}{\epsilon_0} \quad (3.1)$$

Here the original potential function $U(x, y)$ in (1.1) becomes an equivalent function in radial coordinates $\psi(r, \theta)$.

3.1 Problem Construction

Since the solution sought is radially symmetric, the 2D potential function $\psi(r, \theta)$ becomes $\psi(r)$, with the transformed Poisson's equation (3.1) becoming the ODE

$$\frac{1}{r} \frac{d}{dr} \left(r \frac{d\psi(r)}{dr} \right) = -\frac{\rho(r)}{\epsilon_0} \quad (3.2)$$

Similarly to the planar case, the problem outlined in Section 1.2 can now be reduced to the 1D radial problem shown in Figure 3.1. The problem is then

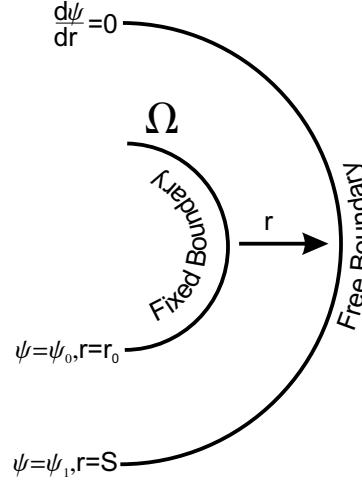


Figure 3.1: 1D Radial problem setup

to find the function $\psi(r)$ that satisfies (3.2) subject to the conditions,

$$\left. \begin{aligned} \psi &= \psi_0, & r &= r_0 \\ \psi &= \psi_1 \\ \frac{d\psi}{dr} &= 0 \end{aligned} \right\} r = S \quad (3.3)$$

Initially, as in the planar case, an expression relating $\rho(r)$ to $\psi(r)$ is required. Since ψ is independent of θ , the relationship (2.3) holds with $x \rightarrow r$

$$\rho(r) = \frac{J}{v(r)} \quad (3.4)$$

where $v(r)$ is given by

$$v(r) = \sqrt{\frac{2q}{m}(\psi_1 - \psi(r)) + v_0^2} \quad (3.5)$$

as in the planar case (2.6). From (3.4) and (3.5), the ODE (3.2) becomes

$$\frac{1}{r} \frac{d}{dr} \left(r \frac{d\psi(r)}{dr} \right) = - \frac{J}{\epsilon_0 \sqrt{\frac{2q}{m}(\psi_1 - \psi(r)) + v_0^2}} \quad (3.6)$$

This nonlinear problem subject to the boundary conditions (3.3) is not solvable analytically, and so we appeal to the equidistribution method introduced in Section 2.3 to determine the solution. In order to do this and as in the planar case we introduce a pseudo time variable τ and rewrite (3.6) as the parabolic equation

$$\frac{\partial \phi}{\partial \tau} = \frac{1}{r} \frac{\partial}{\partial r} \left(r \frac{\partial \phi(r)}{\partial r} \right) + g(\phi) \quad (3.7)$$

where $g(\phi)$ is the negative value of the RHS of (3.6) and the steady state radially symmetric function $\psi(r)$ is now written as the time dependent function $\phi(r, \tau)$. The same assumptions as the planar case for the convergence with time of $\phi(r, \tau)$ to the steady state function $\psi(r)$, are made.

3.2 Mapping from Physical Grid to Logical Grid

Since (3.7) subject to the boundary conditions (3.3) is now a moving boundary problem, we proceed in the same manner as in the planar case by mapping the nodes in the physical region Ω on to a logical region Ξ . Again, forcing the distribution of nodes in the logical region to be constant in time allows the nodal velocities in the physical region to be calculated.

In this case, the monitor function M must be chosen such that¹

$$Mr \frac{dr}{d\xi} = 1 \quad (3.8)$$

Proceeding as before and integrating over the physical solution region,

$$\begin{aligned} \int_{r_0}^{r_n(\tau)} Mr dr &= \int_{\xi_0}^{\xi_n(\tau)} d\xi \\ &= \xi_n(\tau) - \xi_0 \\ &= \Theta(\tau) \end{aligned} \quad (3.9)$$

¹dx in planar geometry becomes rdr in radial geometry.

where $r_n(\tau)$ corresponds to the moving outer boundary (S in Figure 3.1). Also integrating (3.8) over a single 'element' in the physical region gives

$$\begin{aligned} \int_{r_{i-1}}^{r_i} Mr dr &= \int_{\xi_{i-1}}^{\xi_i} d\xi \\ &= \Delta\xi \end{aligned} \quad (3.10)$$

Holding the ratio, $\Delta\xi/(\xi_n(\tau) - \xi_0)$ constant in time

$$\frac{1}{\Theta(\tau)} \int_{r_{i-1}}^{r_i} Mr dr = c_{i-\frac{1}{2}} \quad (3.11)$$

again allows an expression relating the nodal velocities \dot{r} and $\dot{\Theta}$ to be found.

This is done by taking the time derivative of (3.11)

$$\frac{dc}{d\tau} = 0 = \frac{\partial c}{\partial r} \frac{dr}{d\tau} + \frac{\partial c}{\partial \tau} \quad (3.12)$$

with the first term on the RHS of (3.12) being given by

$$\frac{\partial c}{\partial r} \frac{dr}{d\tau} = \frac{1}{\Theta(\tau)} \left[Mr \dot{r} \right]_{r_{i-1}}^{r_i} \quad (3.13)$$

The second term on the RHS of (3.12) may be written

$$\frac{\partial c}{\partial \tau} = \int_{r_{i-1}}^{r_i} \frac{\partial}{\partial \tau} \left(\frac{Mr}{\Theta(\tau)} \right) dr = 0 \quad (3.14)$$

which on expansion gives

$$\frac{\partial c}{\partial \tau} = \frac{1}{\Theta} \int_{r_{i-1}}^{r_i} M \dot{r} dr + \frac{1}{\Theta} \int_{r_{i-1}}^{r_i} \frac{\partial M}{\partial \tau} r dr - \frac{\dot{\Theta}}{\Theta^2} \int_{r_{i-1}}^{r_i} Mr dr \quad (3.15)$$

Combining (3.13) and (3.15),

$$\begin{aligned} \int_{r_{i-1}}^{r_i} M \dot{r} dr + \int_{r_{i-1}}^{r_i} \frac{\partial M}{\partial \tau} r dr \\ - \frac{\dot{\Theta}}{\Theta} \int_{r_{i-1}}^{r_i} Mr dr + \left[Mr \dot{r} \right]_{r_{i-1}}^{r_i} = 0 \end{aligned} \quad (3.16)$$

and approximating the integrals using the trapezium rule once again yields an $(n+1) \times n$ system of equations for the n nodal velocities \dot{r} and $\dot{\Theta}$ ($r_0 = 0$).

Again, since this is not a square system, the mass balance equation relating to the original DE (3.7),

$$\frac{d}{d\tau} \int_{r_0}^{r_n} \phi r dr = \int_{r_0}^{r_n} \left(\frac{1}{r} \frac{\partial}{\partial r} \left(r \frac{\partial \phi(r)}{\partial r} \right) + g(\phi) \right) r dr \quad (3.17)$$

is used to provide a further relationship between the nodal velocities \dot{r} and $\dot{\Theta}$ (see Section 3.4).

3.3 Choice of Monitor Function

The case for the monitor function $M = 1$ is not evaluated here for the reasons given in Section 2.6.1.

If we choose $M = 1 + \frac{\gamma}{r} \phi_r$, then from (3.8)

$$\frac{dr}{d\xi} = \frac{1}{r + \gamma \phi_r}, \quad (3.18)$$

it is clear that if the solution gradient ϕ_r is high, the rate of change of nodes in the physical domain with respect to the logical domain will be small. In addition, as the radial coordinate increases this rate of change will also decrease.

Using this monitor function and from (3.9) and (3.10), the ratio $\Delta\xi/(\xi_n(\tau) - \xi_0)$ is given by

$$\begin{aligned} \frac{\Delta\xi}{\xi_n(\tau) - \xi_0} &= \frac{\frac{1}{2} (r_i^2 - r_{i-1}^2) + \gamma (\phi_i - \phi_{i-1})}{\frac{1}{2} (r_n^2 - r_0^2) + \gamma (\phi_n - \phi_0)} \\ &= c_{i-\frac{1}{2}} \end{aligned} \quad (3.19)$$

If the moving boundary at $r_n(\tau)$ moves in a positive r direction, the denominator of the term on the RHS of (3.19) will increase quadratically. In order that this term remain constant in time, either the i^{th} element solution

difference $(\phi_i - \phi_{i-1})$ must increase, the element size must increase, or a combination of both. For small i , the size of an element will increase more significantly than for large i (for a similar element solution gradient) at each timestep.

Substituting $M = 1 + \frac{\gamma}{r}\phi_r$ into (3.16) gives

$$\begin{aligned} \int_{r_{i-1}}^{r_i} \left(1 + \frac{\gamma}{r}\phi_r\right) \dot{r} dr &= \frac{\partial}{\partial \tau} \int_{r_{i-1}}^{r_i} r dr + \gamma \int_{r_{i-1}}^{r_i} \frac{\dot{r}\phi_r}{r} dr \\ &= [r\dot{r}]_{r_{i-1}}^{r_i} + \gamma \int_{r_{i-1}}^{r_i} \frac{\dot{r}\phi_r}{r} dr \end{aligned} \quad (3.20)$$

for the first term,

$$\begin{aligned} \int_{r_{i-1}}^{r_i} \frac{\partial M}{\partial \tau} r dr &= \gamma \int_{r_{i-1}}^{r_i} \frac{\partial}{\partial \tau} \left(\frac{\phi_r}{r}\right) r dr \\ &= \gamma \int_{r_{i-1}}^{r_i} \phi_{r\tau} - \frac{\dot{r}\phi_r}{r} dr \end{aligned} \quad (3.21)$$

for the second term, and

$$-\frac{\dot{\Theta}}{\Theta} \int_{r_{i-1}}^{r_i} M r dr = -c_{i-\frac{1}{2}} \dot{\Theta} \quad (3.22)$$

for the third term (from (3.11)).

Combining (3.20), (3.21) and (3.22) and substituting into (3.16) gives the expression

$$\underbrace{\gamma \left[\frac{1}{r} \frac{\partial}{\partial r} \left(r \frac{\partial \phi(r)}{\partial r} \right) + g(\phi) \right]_{r_{i-1}}^{r_i}}_{I_1} + [r\dot{r}]_{r_{i-1}}^{r_i} + [(r + \gamma\phi_r)\dot{r}]_{r_{i-1}}^{r_i} - \dots \dots - c_{i-\frac{1}{2}} \dot{\Theta} = 0 \quad (3.23)$$

where the term I_1 comes from the differential equation (3.7) and becomes the RHS of the system (3.23). This system represents the main $(n+1) \times n$ equations in \dot{r} and $\dot{\Theta}$.

The second and third terms in (3.23) may be expanded to give

$$[r\dot{r}]_{r_{i-1}}^{r_i} = r_i \dot{r}_i - r_{i-1} \dot{r}_{i-1} \quad (3.24)$$

$$[(r + \gamma\phi_r)\dot{r}]_{r_{i-1}}^{r_i} = (r_i + \gamma\phi_r|_{r_i}) \dot{r}_i - (r_{i-1} + \gamma\phi_r|_{r_{i-1}}) \dot{r}_{i-1} \quad (3.25)$$

and the term I_1 ,

$$\begin{aligned}
\gamma \left[\frac{1}{r} \frac{\partial}{\partial r} \left(r \frac{\partial \phi(r)}{\partial r} \right) + g(\phi) \right]_{r_{i-1}}^{r_i} &= \gamma \left\{ \frac{1}{r_i} \frac{\partial}{\partial r} \left(r_i \frac{\partial \phi}{\partial r} \Big|_{r_i} \right) \Big|_{r_i} - \dots \right. \\
\dots - \frac{1}{r_{i-1}} \frac{\partial}{\partial r} \left(r_{i-1} \frac{\partial \phi}{\partial r} \Big|_{r_{i-1}} \right) \Big|_{r_{i-1}} &+ \left. g(\phi_i) - g(\phi_{i-1}) \right\} \\
&= -b_i
\end{aligned} \tag{3.26}$$

where the derivatives within (3.26) are approximated as follows:

When $i = 1$,

$$\frac{\partial}{\partial r} \left(r_1 \frac{\partial \phi}{\partial r} \Big|_{r_1} \right) \Big|_{r_1} \approx \frac{r_2 \frac{\partial \phi}{\partial r} \Big|_{r_2} - r_0 \frac{\partial \phi}{\partial r} \Big|_{r_0}}{(r_2 - r_0)} \tag{3.27}$$

using a central difference to approximate the outer derivative.

When $i = 2$ to $n + 1$,

$$\frac{\partial}{\partial r} \left(r_i \frac{\partial \phi}{\partial r} \Big|_{r_i} \right) \Big|_{r_i} \approx \frac{r_{i+1} \frac{\partial \phi}{\partial r} \Big|_{r_{i+1}} - r_{i-1} \frac{\partial \phi}{\partial r} \Big|_{r_{i-1}}}{(r_{i+1} - r_{i-1})}, \tag{3.28}$$

again using a central difference to approximate the outer derivative.

When $i = n$,

$$\frac{\partial}{\partial r} \left(r_n \frac{\partial \phi}{\partial r} \Big|_{r_n} \right) \Big|_{r_n} \approx \frac{r_{n-1} \frac{\partial \phi}{\partial r} \Big|_{r_{n-1}}}{(r_{n-1} - r_n)}, \tag{3.29}$$

using a backward difference to approximate the outer derivative (and noting that $\phi_r|_{r_n} = 0$ from (2.3))

Combining (3.24), (3.25) and (3.26), equation (3.23) may be written as the

system

$$\begin{aligned}
 & \left(\begin{array}{cccccc}
 (2r_1 + \gamma \phi_r|_{r_1}) & 0 & 0 & \cdots & -c_{\frac{1}{2}} \\
 -(2r_1 + \gamma \phi_r|_{r_1}) & (2r_2 + \gamma \phi_r|_{r_2}) & 0 & & -c_{\frac{3}{2}} \\
 \vdots & \ddots & \ddots & & \vdots \\
 0 & & -(2r_{n-1} + \gamma \phi_r|_{r_{n-1}}) & 2r_n & -c_{n-\frac{1}{2}}
 \end{array} \right) \times \cdots \\
 & \cdots \times \begin{pmatrix} \dot{r}_1 \\ \dot{r}_2 \\ \vdots \\ \dot{r}_n \\ \dot{\Theta} \end{pmatrix} = \begin{pmatrix} b_1 \\ b_2 \\ \vdots \\ b_n \end{pmatrix}
 \end{aligned} \tag{3.30}$$

3.4 Application of Mass Balance Equation

Discretising the mass balance equation given in (3.17) and adding this to the system (3.30) will cause the same non-convergence seen in Section 2.9.1. With this in mind, the same correction as is applied in Section 2.9.2 will be applied here, and the mass balance equation is therefore reduced to

$$\begin{aligned}
 \frac{d}{d\tau} \int_{r_0}^{r_n} \phi r dr &= \int_{r_0}^{r_n} \frac{\partial}{\partial \tau} (\phi r) dr + \phi_n r_n \dot{r}_n \\
 &= 0
 \end{aligned} \tag{3.31}$$

noting that $\dot{r}_0 = 0$.

Expanding the first term on the RHS of (3.31) gives

$$\int_{r_0}^{r_n} \frac{\partial}{\partial \tau} (\phi r) dr = \int_{r_0}^{r_n} \underbrace{r \dot{\phi}}_{I_2} + \underbrace{\phi \dot{r}}_{I_3} dr \tag{3.32}$$

where I_2 can be approximated by

$$\begin{aligned}
 \int_{r_0}^{r_n} r \dot{\phi} dr &\approx \frac{1}{2} \sum_{i=1}^n (r_i - r_{i-1}) (r_i \dot{\phi}_i + r_{i-1} \dot{\phi}_{i-1}) \\
 &= \frac{1}{2} \sum_{i=1}^{n-1} (r_{i+1} - r_{i-1}) r_i \dot{\phi}_i
 \end{aligned} \tag{3.33}$$

(noting that $\dot{\phi}_n = 0$) and I_3 by

$$\begin{aligned} \int_{r_0}^{r_n} \phi \dot{r} dr &\approx \frac{1}{2} \sum_{i=1}^n (r_i - r_{i-1})(\phi_i \dot{r}_i + \phi_{i-1} \dot{r}_{i-1}) \\ &= \frac{1}{2} (r_n - r_{n-1}) \phi_n \dot{r}_n + \frac{1}{2} \sum_{i=1}^{n-1} (r_{i+1} - r_{i-1}) \phi_i \dot{r}_i \end{aligned} \quad (3.34)$$

Clearly an expression relating $\dot{\phi}_i$ and $\dot{\Theta}$ is required to obtain a system in \dot{r} and $\dot{\Theta}$ from (3.31). Such an expression can be found by summing (in a similar manner to the planar case) the constant $c_{i-\frac{1}{2}}$ in (3.19),

$$\Theta \sum_{j=i+1}^n c_{j-\frac{1}{2}} = \frac{1}{2} (r_n^2 - r_i^2) + \gamma (\phi_n - \phi_i) \quad (3.35)$$

such that

$$\phi_i = \phi_n - \frac{\Theta}{\gamma} \overline{C}_i + \frac{1}{2\gamma} (r_n^2 - r_i^2) \quad (3.36)$$

where $\sum_{j=i+1}^n c_{j-\frac{1}{2}} = \overline{C}_i$ as before.

Taking the time derivative of (3.36) gives the required expression

$$\dot{\phi}_i = -\frac{\dot{\Theta}}{\gamma} \overline{C}_i + \frac{1}{\gamma} (r_n \dot{r}_n - r_i \dot{r}_i) \quad (3.37)$$

Using (3.33), (3.34) and (3.37) in the mass balance equation (3.31) and collecting terms in \dot{r}_i , \dot{r}_n and $\dot{\Theta}$ gives the final equation to be added to the system (3.30),

$$\begin{aligned} &\frac{1}{2} \sum_{i=1}^{n-1} \left(\phi_i - \frac{r_i^2}{\gamma} \right) (r_{i+1} - r_{i-1}) \dot{r}_i + \frac{1}{2} \left\{ (3r_n - r_{n-1}) \phi_n + \dots \right. \\ &\left. \dots + \frac{r_n}{\gamma} \sum_{i=1}^{n-1} r_i (r_{i+1} - r_{i-1}) \right\} \dot{r}_n - \frac{\dot{\Theta}}{2\gamma} \sum_{i=1}^{n-1} r_i (r_{i+1} - r_{i-1}) \overline{C}_i \\ &= 0 \end{aligned} \quad (3.38)$$

3.5 Results and Conclusions From the Equidistribution Method for Radial Geometry

Inspection of the matrix in (3.30) shows that it has the same bi-diagonal structure as in the planar case. Indeed successive addition of rows will lead to the main bulk of the system becoming diagonal, such that the inversion method detailed in Section 2.8 can be used.

The method of solution proceeds in a similar way to the planar case (Section 2.9) with the exception of the initial condition which was chosen to be the planar analytic solution generated in Section 2.1 (it was expected that this would be close to the radial solution).

3.5.1 Large Solution Region - $J = 0.01Am^{-2}$

Initially we compare the planar analytic solution with the radial solution for the case $J = 0.01Am^{-2}$ and an accelerating potential difference of 100KV (ions are deuterons and have an initial energy of 50eV). Such a relatively small current density is chosen because the calculated solution region width is large ($\sim 11m$ in comparison to $\sim 1m$ for $J = 1Am^{-2}$). Due to this, it is expected that there will be a reasonable difference in solution between the radial and planar geometries. As the solution region width increases, the inner fixed boundary appears more and more like a point charge relative to the free boundary (such that the electric field there increases relative to the remainder of the region), which appears more and more like a plane. It is expected then, that differences in solution between the radial and planar cases for the large solution region will occur primarily towards the fixed boundary.

Figure 3.2 shows the analytic planar solution for these conditions in addition to radial solutions at two different times. As time progresses, the radial solution is moving away from the planar solution initial condition and as expected, differences between the two solutions occur primarily towards the fixed boundary. Figure 3.3 shows the position of the moving boundary for the radial solution which is clearly moving away from the planar free bound-

ary position and converging to a nearby position. Examination of the nodal

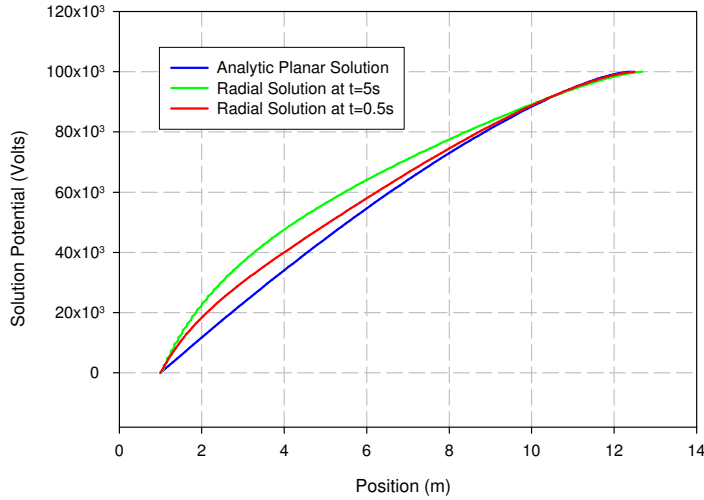


Figure 3.2: Analytic free boundary and radial moving boundary solutions for the conditions $J = 0.01Am^{-2}$ and $(\phi_n - \phi_0) = 100KV$.

positions with time also indicates that convergence is taking place, and that the majority of nodal movement away from the initial condition occurs near to the fixed boundary.

Figure 3.4 shows nodal positions with time for a selection of nodes with equally spaced indices. At time $t = 0$, the nodes are equally spaced in distance (due to the initial analytic planar solution being calculated using an RK4 algorithm), but as time progresses the nodes bunch up at the fixed boundary end. A close inspection of Figure 3.2 indicates that the solution gradient (of the radial solution) near the fixed boundary end of the solution region ($\phi_r \sim 20KVm^{-1}$ near the fixed boundary end) is high relative to the gradient towards the free boundary end of the region ($\phi_r \sim 5KVm^{-1}$ near the free boundary end). Referring to (3.18), this will cause $\frac{dr}{d\xi}$ to be small near the fixed boundary end of the physical solution region hence causing the nodes to bunch up². Figure 3.5 shows the distance the nodes have moved

²The radial position r in (3.18) has little effect since its absolute value is significantly

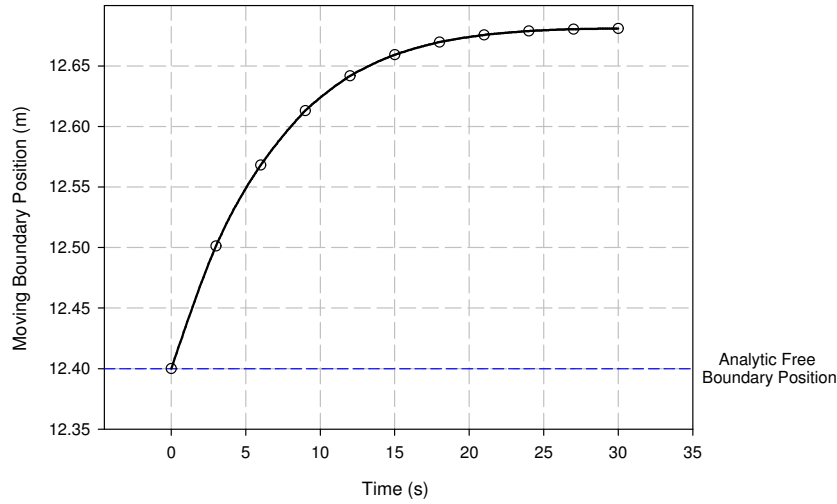


Figure 3.3: Position of moving boundary as a function of time for the radial solution with conditions $J = 0.01Am^{-2}$ and $(\phi_n - \phi_0) = 100KV$.

(relative to their starting position) as a function of time for the same selection of nodes as in Figure 3.4. A close inspection of Figure 3.5 again indicates that the majority of nodal movement occurs close to the fixed boundary.

3.5.2 Variation in Solution Region Size with Emission Current Density

As in the planar case (Section 2.2.1) it is expected that as the current density of the emitter increases (with a constant accelerating potential), the solution region width will decrease. In addition, it is also expected that as the current density increases, the difference between the planar and radial solutions will decrease (for reasons given in Section 3.5.1).

Figure 3.6 is a repeat of Figure 2.3 but with radial and planar solutions included. As expected the solution region does decrease in size with increasing current density at the emitter. In addition, the difference between the smaller than that of the solution gradient.

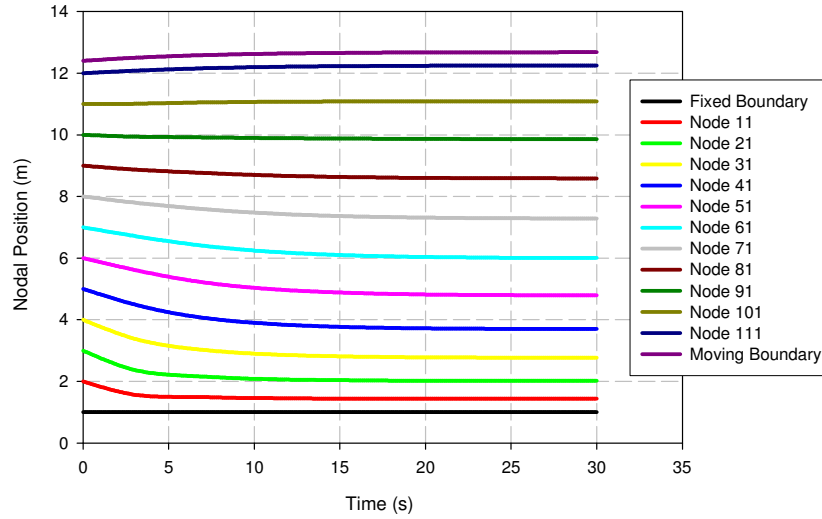


Figure 3.4: Nodal position as a function of time for the condition $J = 0.01Am^{-2}$ and $(\phi_n - \phi_0) = 100KV$.

planar and radial solutions disappears as the current density increases (and hence the solution region width decreases).

3.5.3 Variation in Solution Region Size with Accelerating Potential

Again as in the planar case, it is expected that as the accelerating potential $(\phi_n - \phi_0)$ increases, the solution region will increase in size. This is (as previously explained) due to plasma being more readily stripped away (due to the higher electric field) from the free boundary, therefore causing it to recede. Figure 3.7 is a repeat of Figure 2.5 but with radial and planar solutions included. The solution region width does indeed increase with increasing accelerating potential and as the accelerating potential decreases, the difference between planar and radial solutions disappears.

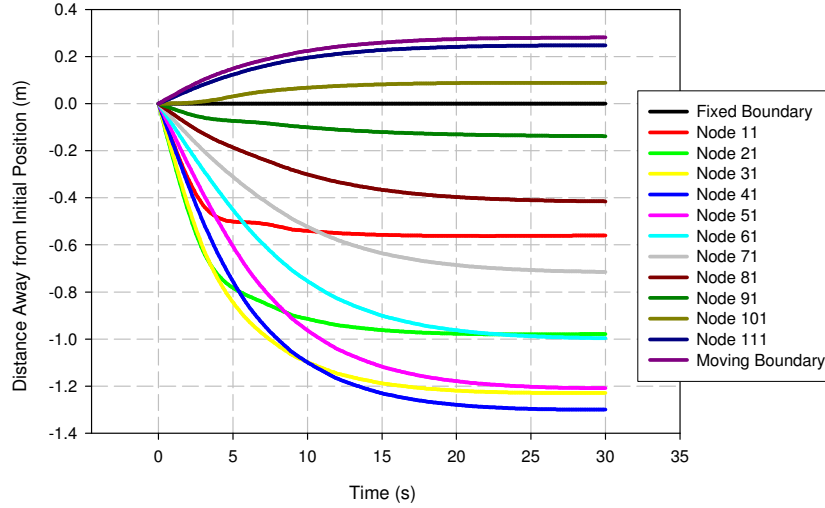


Figure 3.5: Nodal positions relative to their starting point as a function of time (for the condition $J = 0.01Am^{-2}$ and $(\phi_n - \phi_0) = 100KV.$)

3.5.4 The Effect of the Parameter γ

Referring to (3.18), the parameter γ governs the effect the solution gradient ϕ_r has on nodal spacing. As has already been seen in Section 3.5.1 the effect of a high solution gradient appears to be to concentrate nodes in the area of the high gradient.

If γ is of a size $1/\hat{\phi}_r$ where $\hat{\phi}_r$ is the mean gradient over the region, the effect of ϕ_r on the nodal spacing (and nodal velocity at each time step) can be limited. Indeed if γ is sufficiently small, the effect of ϕ_r on the nodal spacing can be removed altogether. We now investigate the effect of γ on a test problem.

By the mean value theorem, at at least one point c within the solution region the solution gradient will be given by

$$\phi_r(c) = \frac{\phi_n - \phi_0}{r_n - r_0} \quad (3.39)$$

provided the solution is continuous and differentiable across the region. Re-

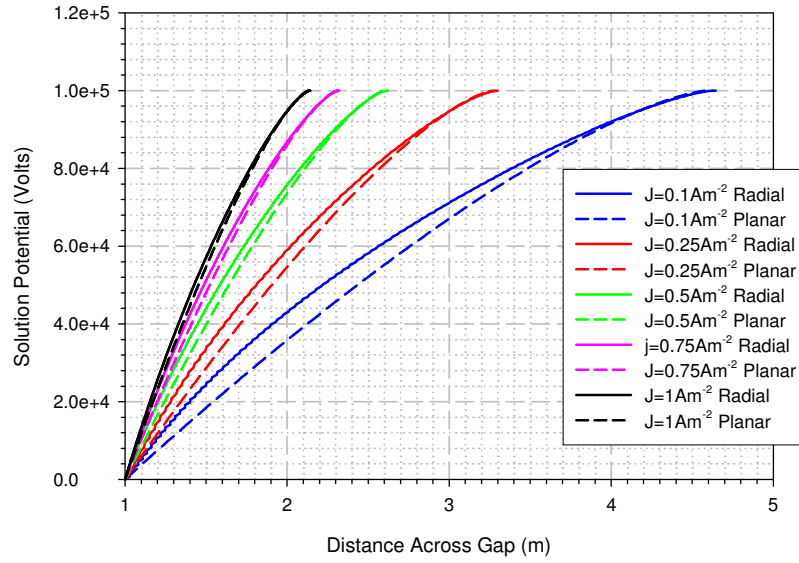


Figure 3.6: Variation in potential across the solution region for different emission current densities.

ferring to Figure 3.2 (100KV , 0.01Am^{-2}) the solution gradient will therefore take the value $\phi_r \sim 8.5\text{KVm}^{-1}$ at some point within the solution region (which has a width of 11.68m for this accelerating potential and current density in radial geometry). In order to show the effect of changing the parameter γ , the nodal positions with time for this particular solution, are calculated for varying values of γ .

Figure 3.8 shows the nodal positions with time for nodes in the region near to the fixed boundary (nodes between 2m and 6m in Figure 3.4, 100KV , $J = 0.01\text{Am}^{-2}$) where the majority of nodal movement is observed. When γ is increased from 1 to 100000 , there is little effect since the value of the ratio on the RHS of (3.18) with the mean solution gradient quoted above is already very small. Increasing γ serves to cause the derivative on the LHS to become closer to zero, with little net effect on the nodal spacing.

It is expected that due to the size of the mean solution gradient, γ must be reduced to ~ 0.001 to have a significant effect. It was not possible to

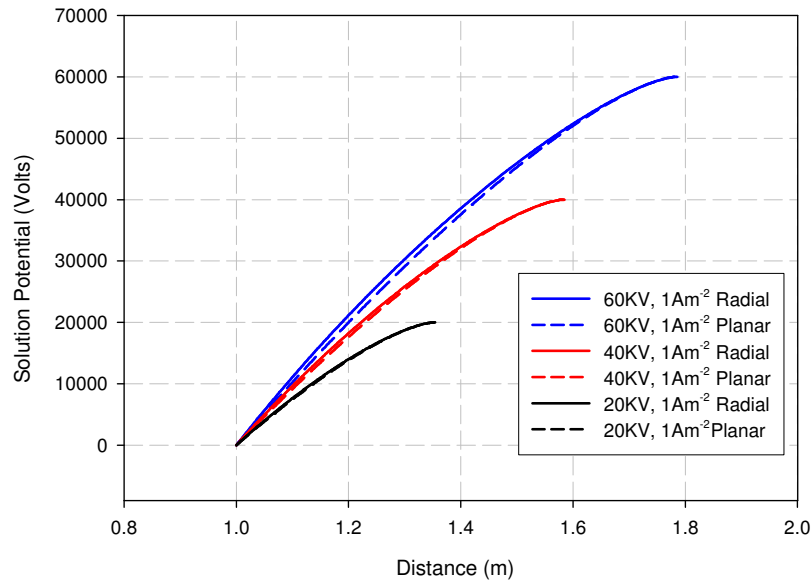


Figure 3.7: Change in solution potential with distance for varying solution region potential differences.

reduce γ to this value in practise as the calculation failed. This is most likely due to the presence of γ in (3.36) and (3.37) causing large solution changes with time. However, γ was set at a value of 0.007 which when multiplied by the mean solution gradient given above reduces this product to a similar order of magnitude to the variable r , hence increasing the RHS of (3.18). Close examination of Figure 3.8 does show that there is slightly less nodal movement with time for those nodes displayed with this value of γ .

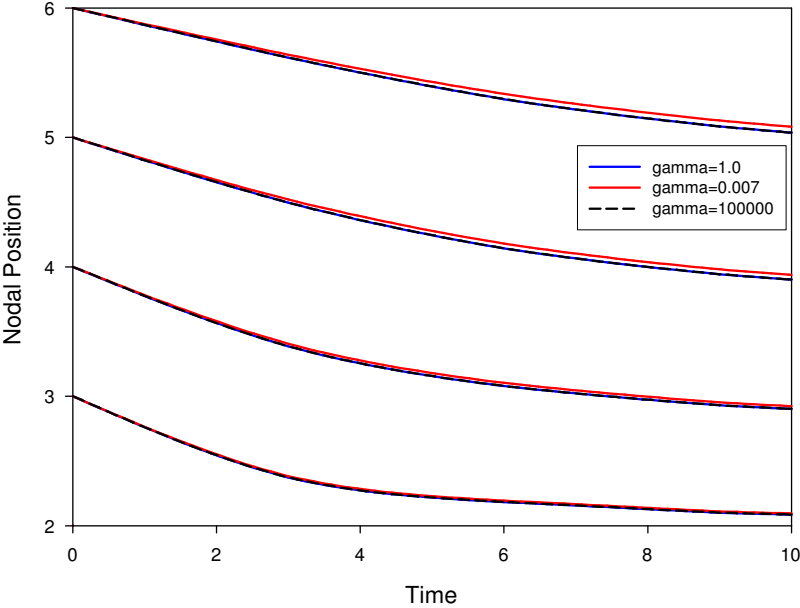


Figure 3.8: The effect of γ on nodal movement.

Chapter 4

Conclusions and Further Work

4.1 Conclusion

The problem of determining the position of the plasma boundary formed between an expanding plasma and a large electric field was constructed and initially solved (in the most part analytically) for the 1D planar case.

Exploration of the solution to this problem revealed that the behaviour of the solution and boundary position as a function of various initial conditions (such as accelerating voltage and current density) was exactly as expected.

We confirmed that the solution region width reduces in size as the ion emission current density increases. In a physical sense, this is due to the increase in ion flux reaching the plasma boundary being greater than the ion flux being stripped away from the boundary by the accelerating electric field. As such, the plasma bulges into the region, reducing it in size, until the electric field is sufficiently high that the ion flux both reaching and leaving the boundary are balanced. This is the equilibrium state and is the position of the free boundary.

In addition we confirmed that as the accelerating voltage is reduced in magnitude, the solution region size reduces. This is again due to the ion flux reaching the plasma boundary being greater than the flux caused by ions being stripped away by the (reduced) electric field. The solution region con-

sequently reduces in size until the ion fluxes on both sides of the boundary are balanced.

Since one of the aims of this project was to solve the same problem in a 1D radially symmetric geometry and it was apparent that this radial problem could not be solved in the same analytic way as the planar case, a new iterative method of solution was constructed. The method was initially applied to the same 1D planar case.

In order to apply the iterative method, the problem was modified to include an artificial time dependence. It was assumed that the solution of this new moving boundary problem would converge to the solution of the original fixed boundary problem as time proceeds to infinity. This assumption was not explicitly proven.

Initially it was found that the correct convergence did not take place, and that this was due to the application of the mass balance equation to an initially time independent problem where the position of the moving boundary is implicitly defined. Convergence was achieved by setting the RHS of the mass balance equation to be equal to zero which had the effect of fixing the solution 'mass' in time.

Confident that the iterative method was working in planar geometry, we applied the method to the equivalent 1D radially symmetric problem. Studies into the solution of this problem indicated that it also behaved as expected, and a closer investigation into the numerical method indicated that solution nodes were also moving in an expected way as time stepping proceeded.

As far as we know, this work is new.

4.2 Further Work

4.2.1 Convergence

By converting the original time independent free boundary problem to a parabolic moving boundary problem, it has been assumed that the same equilibrium solution would be ultimately obtained in both cases. We would like to be able to show analytically that this is indeed the case.

4.2.2 Stability

During many runs of the iterative numerical method, it was noted that certain step sizes, time step sizes, current densities, and affected the stability of the method. Indeed it would be expected that due to the difference approximations employed within the method, an increased step length would adversely affect stability (and accuracy). It would therefore be pertinent to investigate the stability of the method in relation to these input parameters.

Acknowledgements

I would like to acknowledge Professor Mike Baines for his unending knowledge of this subject, and without whose help this project would have been significantly more difficult! I would like to thank AWE plc, and in particular Dave Deas and Ian Marshall of the Neutron Generator department. Without their generosity in time and support, this project and indeed this MSc would not have been possible. I would also like to thank Sue Davis for our many chats and for her words of support, in addition to the friends I have made within the Maths Department at Reading University. Finally I would like to thank my partner Thelma for putting up with me and suffering all those nights alone as a computer widow. By doing this she was helping me the best way she could.

Bibliography

- [1] Karl R Spangenburg. *Vacuum Tubes*, McGraw Hill, 1948
- [2] M J Baines *et al.* Adaptive FE Solutions of Time Dependent Partial Differential Equations Using Moving Mesh Algorithms, *Proceedings to Modelling and Simulation in Chemical Engineering, Coimbra, Portugal*, 3rd Article, June 30 - July 4 2003.
- [3] M J Baines. A Lagrangian Moving Finite Element Method Incorporating Monitor Functions, *Proceedings of SCA03 Conference, Hong Kong*, Jan 2003.
- [4] John Crank. *Free and Moving Boundary Problems*, Clarendon Press, 1984
- [5] P J Spence. Use of Adaptive Grid Methods in the Solution of a 1D Second Order ODE, *AWE Internal Memo No. AWE/DWE20/98/S6048*, UK UNCLASSIFIED, 1998